

# TENSOR VECTOR FIELD BASED ACTIVE CONTOURS

*Abhishek Kumar, Alexander Wong, Akshaya Mishra, David A. Clausi, and Paul Fieguth*

Department of Systems Design Engineering  
University of Waterloo  
Waterloo, Canada

## ABSTRACT

Among the main limitations of active contours are their high noise sensitivity and poor capture range from the target object. One of the most promising approaches for addressing these limitations is the concept of Vector Field Convolution (VFC). However, due to its isotropic vector field kernel, VFC does not take full advantage of the underlying image structural characteristics. By specifically addressing this idea, a novel local tensor vector field approach is developed to adaptively account for these structural characteristics. Experimental results demonstrate that the proposed adaptive method leads to more accurate segmentation.

**Index Terms**— Active Contour, Snake, Segmentation, Tensor Vector Field, Vector Field Convolution

## 1. INTRODUCTION

Active contours [1, 2, 3] are a set of methods for identifying the boundary of an object of interest in a given image, which is useful for a wide variety of applications in computer vision and medical imaging, such as object tracking and image segmentation. The prime advantage of active contours lies in their implicit way of handling object deformation based on image gradients and other priors.

Briefly, for an active contour, the contour is initialized around the object, following which the contour moves iteratively toward the boundary of the object of interest by minimizing some objective function, ideally eventually fitting itself around the object. The objective function to be minimized has two so-called energy components [1]: i) an internal energy, which constrains the shape of the contour, thus allowing only certain permissible deformations in the contour, and ii) an external energy, which pulls the contour towards the object boundary by favouring gradients or other image features.

The main challenge for an active contour algorithm is to converge a contour to the ideal object boundary irrespective of its initialized shape and position. The algorithm proposed by

Kass et. al. [1] does not effectively capture objects when the initial contour is placed far from the boundary. Furthermore, this approach is very sensitive to the presence of noise in an image, which tends to distract a converging contour from reaching the ideal object boundary by distracting the external energy with high gradients induced by the noise points.

To address these issues, there has been a long history of proposing variations of external fields to improve the convergence of active contours, particularly for contours with concave boundary sections. External fields based on natural force models such as gravitational force based field [4] and electrostatic force [5] have been explored to better move contour points towards the object boundary.

The Gradient Vector Field (GVF) and its more generalized version [6, 3] was introduced to address the issue of the small capture range of the original active contour [1]. GVF addresses the problem of small capture range very effectively and can diffuse the field toward the concave boundary of an object. However, the GVF is both sensitive to noise and is computationally expensive. While there have been improvements to the GVF model [7, 8], they have not yet addressed these limitations effectively.

The Vector Field Convolution (VFC) [9, 10] was proposed to handle the aforementioned limitations of GVF. While VFC has been shown to be more effective than previous external field models at handling noise and improving capture range, it fails to take full advantage of the underlying structural characteristics of the object boundary due to its isotropic property, and still faces difficulty in handling high noise scenarios.

In this paper, we present a novel external field model called Tensor Vector Field (TVF), which adaptively enforces the external field around strong structural characteristics, and hence makes it more robust to noise. In TVF, a vector field kernel is adaptively modified based on the local tensors, helping to generate a smoother and stronger external field by nullifying the distracting affects of noise, leading to faster convergence.

## 2. BACKGROUND

There are two types of active contours: parametric [1, 9, 6] and non-parametric [2]. In this paper, we shall focus on para-

---

Geomatics for Informed Decisions (GEOIDE) and Discovery Grants, both funded by Canada's Natural Science and Engineering Research Council (NSERC), as well as Ontario Centers of Excellence (OCE) are thanked for project funding.

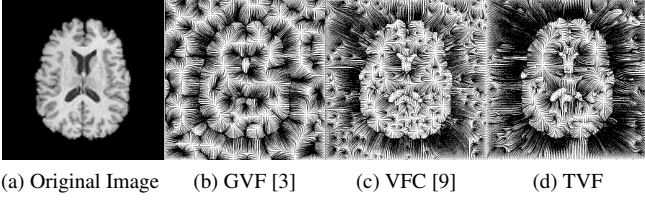


Figure 1: (b, c, d) depict the field streamlines for three different external fields in the brain ( $100 \times 100$  size) image (a), corrupted by impulsive noise. The extent of the desired dark regions [9], shows the effectiveness of the corresponding field in pulling an active contour towards the object boundary.

metric active contours, which can be expressed in terms of a normalized arc length parameter  $s$  as  $c(s) = [x(s)y(s)]$   $s \in [0, 1]$ , where  $x(s)$  and  $y(s)$  are the co-ordinates of the contour in terms of  $s$ . The contour  $c$  deforms with the iterative minimization of its energy  $E_{AC}$ :

$$E_{AC} = \int_0^1 [E_{int}(c(s)) + E_{ext}(c(s))] ds \quad (1)$$

where  $E_{int}$  is the internal energy and  $E_{ext}$  is the external energy. The internal energy  $E_{int}$  is commonly expressed in terms of two components as  $E_{int} = \frac{1}{2}(\alpha|c'(s)|^2 + \beta|c''(s)|^2)$  and works to restrict the shape of the contour, based on some prior model, here constrains on contour stretchability and curvature. The external  $E_{ext}$  drives a contour towards the object boundary and may depend on properties such as intensity, color, gradient etc. As such, the capture range of a contour depends on  $E_{ext}$ .  $E_{AC}$  is minimized by satisfying Eq. 2, obtained by partial differentiation of  $E_{AC}$  (Eq. 1) with respect to  $s$  and equating the result to zero.

$$\underbrace{\alpha c''(s) - \beta c''''(s)}_{F_{int}} - \underbrace{\Delta E_{ext}}_{-F_{ext}} = 0 \quad (2)$$

The deformable contour moves towards the object boundary in order to balance these opposing forces. Figs. 1 and 2 show the external fields created by both GVF and VFC, showing how a particle would move when placed in the field. For visualization, we have shown only those fields which can lead a particle to the object boundary.

In a VFC based external field, the vector field kernel  $\mathbf{k}$  of size  $a \times a$  is defined as  $\mathbf{k} = \mathbf{n}(i, j)m(i, j)$ , where,  $i, j$  are the coordinates with respect to the kernel's center,  $\mathbf{n}(i, j)$  is a unit vector which points to the center of the kernel,  $m(x, y)$  is the magnitude of the vector.  $\mathbf{n}$  and  $m$  can be defined as,

$$\mathbf{n}(i, j) = [-i/r, -j/r] \quad (3)$$

$$m(i, j) = (r + \epsilon)^{-\zeta} \text{ or } m(i, j) = \exp -\frac{r^2}{\sigma} \quad (4)$$

where  $r = \sqrt{i^2 + j^2}$ ,  $\epsilon$  is a small quantity to avoid  $\mathbf{n}(0, 0)$  from tending to infinity,  $\zeta$  and  $\sigma$  are positive values to define the decay of  $m$  as we move away from the origin.

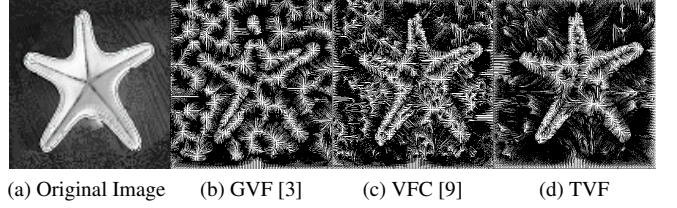


Figure 2: Three field streamlines are shown (b, c, d) corresponding to the starfish ( $109 \times 104$  size) image(a) corrupted by noise. The greater extent of dark regions in (2d) shows the promise of the proposed TVF approach.

$F_{ext}$  is obtained by convolving the edge map  $f(x, y)$  of an image with the kernel  $\mathbf{k}$ . Structural characteristics lead to greater values in  $f$  when compared to uniform regions, thus resulting in a stronger field around strongly structured areas. The capture range clearly depends on the kernel size and decay parameters, so the kernel size is chosen based on the expected or desired capture range of  $F_{ext}$ . One limitation of VFC is that it does not differentiate strong continuous structural characteristics such as the object boundary from random structural fragments due to noise. Therefore, in spite of its robustness compared to other external fields, VFC may still fail to converge in the presence of noise.

### 3. TENSOR VECTOR FIELD

To address the limitations of VFC when dealing with the presence of noise, the concept of structure tensors [11] is incorporated into the construction of the external field in the proposed TVF approach. Structure tensors allow for the characterization of both the direction and coherence of structural characteristics in the image, making it a perfect fit for incorporating structural characteristics. The proposed TVF approach presents a way to improve active contours result by adaptively modifying the VFC kernel using image tensors  $\Gamma(x, y)$ .  $\Gamma(x, y)$  can be expressed as,

$$\Gamma_{x,y} = \begin{pmatrix} \sigma_{x,x} & \sigma_{x,y} \\ \sigma_{y,x} & \sigma_{y,y} \end{pmatrix} \quad (5)$$

where  $\sigma_{x,x}$ ,  $\sigma_{y,y}$  are weighted variances and  $\sigma_{x,y}$  is a weighted covariance of the image gradient. A Gaussian mask of size  $\kappa \times \kappa$  is used to compute these variance and covariance variables. If the mask's center is at the  $x, y$  position of the image, and  $i, j$  are co-ordinates with respect to mask's center, the co-variance of an image gradient can be expressed as

$$\sigma_{x,y} = \sum_{i=-\kappa/2}^{\kappa/2} \sum_{j=-\kappa/2}^{\kappa/2} g(i, j)u_x(i, j)u_y(i, j)$$

where  $g(i, j)$  is an element of the Gaussian mask at  $(i, j)$ ,  $u_x$  and  $u_y$  are image gradients in  $x$  and  $y$  directions respectively.

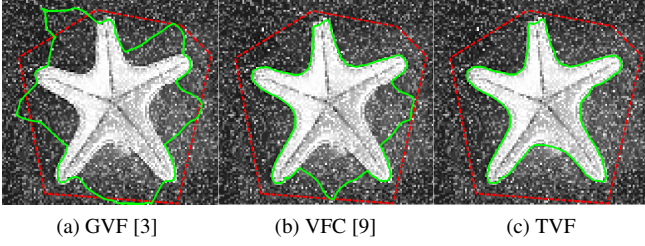


Figure 3: The result of applying active contours to the starfish image (PSNR=25.5 dB) for 30 iterations using three different external field approaches. The red and green curves represent initial and final contours, respectively.

Other weighted variances ( $\sigma_{x,x}$ ,  $\sigma_{y,y}$ ) of the image gradient can be computed in a similar manner. We have used the FFT to accelerate the computation of weighted co-variances and variances. For each  $\Gamma(x, y)$ , the major axis is obtained by calculating a major eigenvector  $\mathbf{v}_+(x, y)$  corresponding to its maximum eigenvalue  $\lambda_+(x, y)$ . As such,  $\mathbf{v}_+(x, y)$  gives the direction along the gradient at  $(x, y)$  and the corresponding  $\lambda_+(x, y)$  gives the gradient strength.

In TVF, the magnitude of each element of the vector field kernel  $\mathbf{k}$  is modified using these major eigenvectors  $\mathbf{v}_+(i, j)$ . Furthermore,  $|\mathbf{n}(i, j)|$  is modified in proportion to the magnitude of the projection of  $\mathbf{v}_+(i, j)$  on the vector kernel element,  $\mathbf{n}(i, j)$ . Therefore, if  $\mathbf{v}_+(i, j)$  is perpendicular to the kernel element vector, the magnitude of that vector element will become zero. The kernel element can thus be modified as

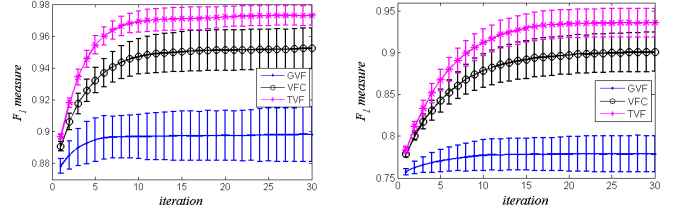
$$\mathbf{k}_{mod}(i, j) = |\mathbf{n}(i, j) \cdot \mathbf{v}_+(i, j)| m(i, j) \lambda_+(i, j) \mathbf{n}(i, j). \quad (6)$$

Finally, the vector field kernel is computed adaptively based on the local tensors, as expressed in Eq. 6. The resulting external field is the desired TVF. Eq. 2 is then solved iteratively using the identical finite difference approach, as used in the VFC method [9].

#### 4. RESULTS AND ANALYSIS

The TVF method is tested on different images with varying amounts of additive Gaussian noise, and the results are compared with that of VFC [9] and GVF [3]. The performance comparison is made consistent by using the same initial contour for each image. The kernel size ( $a$ ), mask size ( $\kappa$ ) and standard deviation of the Gaussian mask have been kept 65, 5 and 1, respectively. A commonly used segmentation performance comparison parameter, the  $F_1$  measure [12], is used to compare the results of the three active contour results. The measure is expressed as

$$F_1 \text{ measure} = \frac{2 \times \text{precision} \times \text{recall}}{\text{precision} + \text{recall}} \quad (7)$$



(a) Brain (Fig. 1a), PSNR = 25.2 (b) Starfish (Fig. 2a), PSNR = 25.4

Figure 4: Convergence behaviour of the active contour for all three external fields. The proposed TVF converges in approximately the same number of iterations as VFC, but with a higher  $F_1$  measure.

where precision =  $\frac{TP}{TP+FP}$  and recall =  $\frac{TP}{TP+FN}$ .  $TP$ ,  $FP$ , and  $FN$  represents the area of true positive regions, false positive regions, and false negative regions, respectively, where each area is computed as a pixel count.

In Fig. 1, the higher density and the even distribution of the dark regions allow for better likelihood of convergence [9]. We can clearly observe that TVF does better than VFC and GVF in satisfying this criterion. A similar pattern, showing the stronger performance of TVF over VFC, GVF can be observed in Fig. 2.

Fig. 3 shows the final active contour results after 30 iterations for a low PSNR starfish image (Fig. 2a). It can be observed that the object boundary coincides well with the final contour using TVF, whereas it fails partially for VFC and performs poorly for GVF. This demonstrates the robustness of TVF to noise. In high PSNR scenarios, due to the absence of noise distraction, both TVF and VFC give similar performance. TVF shows improvements for both concave and convex types of boundaries.

Fig. 5 shows a comparison using the  $F_1$  measure for the starfish image after 30 iterations under different PSNR scenarios. Twenty iterations of each algorithm were run on a set of images with randomly induced Gaussian noise. The plot clearly shows that TVF outperforms the other tested algorithms. Figs. 4a and 4b show that TVF takes almost the same number of iterations to converge to the object boundary. Moreover, the standard deviation of the  $F_1$  measure is smaller for TVF, indicating greater stability. Table 1 shows the comparative results for VFC, GVF, and TVF using different types of images. TVF outperforms the other tested methods in all the cases. While TVF is slower than VFC, it can be useful in noisy situations, specially when the object boundary is prominent and the noise is random.

#### 5. CONCLUSION

We have introduced a novel tensor vector field (TVF), to be used in active contours based image segmentation. This

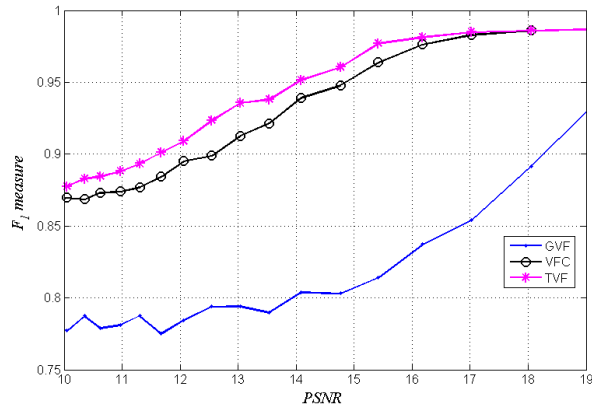


Figure 5: A comparison of the proposed TVF field with VFC and GVF. TVF matches or exceeds the performance of VFC and GVF for a wide range of PSNR scenarios.

model uses an adaptive vector field kernel based on local tensor information to better utilize the underlying image structural characteristics and promote convergence in fewer iterations. Different comparisons clearly shows that TVF provides improved performance over earlier external fields VFC and GVF in terms of both accuracy and stability when faced with noise contaminated situations.

## Acknowledgement

We would like to thank authors of [9] for providing the VFC code, which was very useful in generating results of this paper.

## 6. REFERENCES

- [1] M. Kass, A. Witkin, and D. Terzopoulos, “A snakes-active contour models,” *International Journal of Comp. Vision*, vol. 1, pp. 321–331, 1987.
- [2] T. Chan, B. Sandberg, and L. Vese, “Active contours without edges for vector-valued images,” *J. Visual Comm. and Image Representation*, vol. 11, pp. 130–141, 2000.
- [3] C. Xu and J. L. Prince, “Generalized gradient vector flow external forces for active contours,” *Signal Processing*, vol. 71, pp. 131–139, December 1998.
- [4] F. Shih and K. Zhang, “Locating object contours in complex background using improved snakes,” *Computer Vision Graphics and Image Understanding*, vol. 105, pp. 93–98, 2007.
- [5] A. Jalba and M. Wilkinson and J. Roerdink, “Cpm: A deformable model for shape recovery and segmentation based on charged particles,” *IEEE Trans. Pattern Anal. Mach. Intell.*, vol. 26, pp. 1320–1335, October 2004.
- [6] C. Xu and J. L. Prince, “Snakes, shapes, and gradient vector flow,” *IEEE Trans. Image Process*, vol. 7, pp. 359–369, March 1998.
- [7] A. R. Mansouri, D. P. Mukherjee, and S. T. Acton, “Constraining active contour evolution via lie groups of transformation,” *IEEE Trans. Image Process.*, vol. 13, pp. 853–863, June 2004.
- [8] N. Paragios, O. Mellina-Gottardo, and V. Ramesh, “Gradient vector flow fast geometric active contours,” *IEEE Trans. Pattern Anal. Mach. Intell.*, vol. 26, pp. 402–407, March 2004.
- [9] B. Li and S.T. Acton, “Active contour external force using vector field convolution for image segmentation,” *Image Processing, IEEE Trans. on*, vol. 16, pp. 2096–2106, August 2007.
- [10] T. Radulescu and V. Buzuloiu, “Extended vector field convolution snake for highly non-convex shapes segmentation,” *Information Tech. and Applications in Biomed., 9th International Conference on*, pp. 1–4, nov 2009.
- [11] R. L. Garca, R. Deriche, and C. A. Lopez, “Texture and color segmentation based on the combined use of the structure tensor and the image components,” *Signal Processing*, vol. 88, pp. 776–795, April 2011.
- [12] A. K. Mishra, P. W. Fieguth, and D. A. Clausi, “Decoupled active contour (dac) for boundary detection,” *Pattern Anal. Mach. Intell., IEEE Trans. on*, vol. 33, pp. 310–324, 2011.



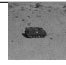


Image	PSNR	$F_1$ measure		
		GVF [3]	VFC [9]	TVF
	25.4	0.79 $\pm 0.022$	0.90 $\pm 0.024$	0.93 $\pm 0.017$
	25.2	0.90 $\pm 0.017$	0.95 $\pm 0.013$	0.97 $\pm 0.006$
	25.3	0.92 $\pm 0.013$	0.97 $\pm 0.009$	0.98 $\pm 0.001$
	25.9	0.85 $\pm 0.022$	0.93 $\pm 0.028$	0.97 $\pm 0.021$
	25.2	0.84 $\pm 0.035$	0.92 $\pm 0.021$	0.96 $\pm 0.026$

Table 1: A comparison of  $F_1$  measure (mean  $\pm$  standard deviation) at the end of 30 iterations for different images, contaminated with Gaussian noise.